Revision 1

FTIR Spectroscopy of D_2O and HDO Molecules in the *c*-axis Channels of Synthetic Beryl

Rudolf I. Mashkovtsev,[1]* Viktor G. Thomas,[1] Dmitry A. Fursenko,[1] Elena S. Zhukova,[2,3] Vladimir V.Uskov,[2] Boris P. Gorshunov[2,3]

[1]V.S. Sobolev Institute of Geology and Mineralogy SB RAS, 630090 Novosibirsk, Russia

[2] Moscow Institute of Physics and Technology, Dolgoprudny, Moscow Region, Russia

[3]A.M. Prokhorov General Physics Institute RAS, Moscow, Russia

*E-mail: rim@igm.nsc.ru

ABSTRACT

This paper presents the results of Fourier transform infrared (FTIR) spectroscopy of a synthetic beryl, containing D_2O molecules in its *c*-axis channels, which we synthesized under hydrothermal conditions at 600 °C and 1.5 kbar. The frequencies of absorbance bands in the range of the stretching vibrations and their overtones and combination modes for D_2O and HDO molecules have been assigned for the first time. On the base of our assignments the absorbance bands observed for the natural beryl in the range of the OD stretching vibrations have been explained.

Keywords: Beryl, emerald, FTIR spectroscopy, H_2O, D_2O and HDO molecules

INTRODUCTION

The nature of water entering into the structure of beryl has attracted the attention of researchers for more than half a century (Wood and Nassau 1967 and Refs therein). Beryl, with ideal formula $Al_2Be_3(Si_6O_{18})$, crystallizes in a hexagonal structure with space group *P*6/*mcc*

(D_{6h}^2). Its honeycomb structure consists of six-membered rings $(Si_6O_{18})^{12-}$ linked together by tetrahedrally coordinated Be ions and octahedrally coordinated Al ions. These six-membered rings are stacked one above the other, forming channels parallel to the *c*-axis (hereafter *c*-channels). These channels are formed by cavities approximately 5.1 Å in diameter, which are separated by "bottlenecks" of 2.8 Å in diameter. There are two types of structural positions in *c*-channels: position 2*a*, with 62 (D_6) symmetry in the center of cavity surrounded by 24 oxygen atoms; and position 2*b*, with 6/m (C_{6h}) symmetry in the center of a six-membered ring. The distance between two neighboring cavities is about 4.6 Å along the *c*-channel. The width of these cavities is sufficient to incorporate single molecules of H_2O, CO_2, N_2, and HCl, as well as ions of NH_4^+, and inert gases of He and Ar (Damon and Kulp 1967; Mashkovtsev and Solntsev 2002; Mashkovtsev and Smirnov 2004; Mashkovtsev and Thomas 2005; Wahler 1956; Wood and Nassau 1967; Zimmerman et al. 1997).

H_2O molecules in the *c*-channels have been mainly classified as type I or type II water with their twofold axis perpendicular or parallel to the crystal *c*-axis, respectively (Wood and Nassau 1967). Normal (unsubstituted or weakly substituted) beryl shows an almost exclusive presence of type I water, whereas type II water becomes dominant when cationic substitution, in four-fold or six-fold coordination, and the content of Li and Na increases (Aines and Rossman 1984; Aurisicchio et al. 1994; Charoy et al. 1996; Łodzinski et al. 2005; Della Ventura et al. (2007). It has been found that an H_2O molecule adjacent to an alkali ion may change its orientation from perpendicular to parallel, due to the effect of the electric field of the charged alkali ion. However, there are currently no clear definitions for the frequencies of type II water molecule stretching bands and type I molecule symmetric band ν_1 as summarized in the tables compiled by Charoy et al. (1996) and Makreski and Jovanvski (2009). Fukuda and Shinoda

(2009) distinguished between type II water molecules coordinated by single or double sodium ions based on ν_1 and ν_2 frequency shifts. The findings of Fukuda and Shinoda (2009) were supported by the study of Della Ventura et al. (2015) who added the data on ν_3 frequency shift. In flux-grown emerald Bellatreccia et al. (2008) studied exclusively type II water molecules that are probably associated with Li impurities.

There are only a few publications (De Donato et al. 2004; Manier-Glavinaz et al. 1989; Zwaan et al. 2012) that have studied D_2O molecules in the *c*-channels of beryl by infrared (IR) spectroscopy. The two stretching modes at 2744 and 2630 cm^{-1} were ascribed to the type I D_2O molecule based on the experiments with natural beryl powder treated with DCl solutions (Manier-Glavinaz et al. 1989). The IR spectra of D_2O and HDO molecules in beryl single crystals with the natural isotopic abundance were observed by De Donato et al. (2004) and Zwaan et al. (2012) but no complete assignment of the OD bands in the stretching-vibration region was done.

Zhukova et al. (2014) and Gorshunov et al. (2013), who explored the dynamics of H_2O molecules confined in the structural channels of beryl using terahertz-infrared spectroscopy, proposed a model, explaining the fine structure of the observed infrared absorption bands. In order to test the validity of this model, we synthesized a unique type of beryl single crystals, containing D_2O in place of H_2O molecules. We aim here to assign the infrared absorbance bands of D_2O and HDO molecules in the *c*-channels of beryl using FTIR spectroscopy.

EXPERIMENTAL METHODS

H_2O, D_2O and HDO bearing beryls were synthesized by the hydrothermal method of Thomas and Klyakhin (1987). Three crystals #3855, #3871 and #3875 with dimensions about 1

× 2 × 3 cm were grown on the seed plates from oxides at 600 °C and 1.5 kbar in a hermetically sealed gold vessel. All reagents were at or higher than 99.8 % pure. Double distilled water and high-purity (99.9 wt %) D_2O were used. The uptake of D_2O molecules by the structural channels during growth was controlled by the molar ratio H/D in hydrothermal media, which was selected at ~1/20 for the samples #3871 and #3875. The compositions of the as-grown crystals were analyzed by wet chemistry with three independent determinations of the oxides (in each case the relative error was not higher than 1% with the detection limit of 0.01 wt %). The results of wet-chemical analyses and the structural formulae (based on 18 O atoms per formula) are listed in Table 1. The Si, Be and Al contents in all studied samples are close to the stoichiometric values. In contrast to channel position of Na^+ the Li^+ occurs both as a framework constituent (replacing Be^{2+} in tetrahedral coordination) and as a channel species at the 2*b* position (Adamo et al. 2008; Sherriff et al. 1991). The Cu^{2+} ions are considered to locate at the tetrahedral Be site in small proportion (see, for example, Adamo et al. 2008 and Refs therein). Table 1 shows the H_2O content of synthetic beryl is similar to those of its natural counterparts (Charoy et al. 1996; Fukuda and Shinoda 2008; Łodzinsky et al. 2005).

The oriented sections parallel to *c*-axis were cut and polished from single crystals using the external morphology as a guide. Polarized FTIR absorption spectra parallel or perpendicular to the *c*-axis were measured at room temperature on a Bruker Vertex 70 FTIR spectrometer equipped with a Hyperion 2000 microscope in the range from 1000 to 7500 cm^{-1} with resolution of 2 cm^{-1}. Polarization of the infrared radiation was achieved using a holographic wire grid polarizer on a ZnSe substrate (Optometrics Corporation, USA).

RESULTS

IR spectra of H_2O molecules. Figure 1 compares the polarized IR absorption spectra in a natural emerald from the Urals and a synthetic hydrothermal beryl #3855. The absorbance is normalized to a sample thickness of 1 cm. For the **E**||*c* polarization the ν_3 mode of type I and the ν_1 and ν_2 modes of type II molecules are IR-active (Wood and Nassau 1967) and are observed at approximately 3700, 3600, and 1630 cm^{-1}, respectively (Fig. 1 and 2). For the **E**⊥*c* polarization the ν_3 mode of type II and the ν_1 and ν_2 modes of type I molecules are IR-active (Wood and Nassau 1967). These two beryl crystals show some differences in their IR spectra, especially for the **E**⊥*c* polarization. The shifts in the frequencies of the ν_3 modes of type II molecules and in combination frequencies involving the libration mode are observed (Table 2). The ν_3 mode for synthetic beryl and natural emerald is observed at 3671 cm^{-1} and at 3660 cm^{-1}, respectively. In natural emerald the band at 2360 cm^{-1} is related to the CO_2 molecule in the *c*-channel (Wood and Nassau 1967). Also, two bands at 2920 and 2850 cm^{-1} are attributed to hydrocarbon groups from the glue that was stuck in the microfissures during grinding to make the very thin beryl plate.

IR spectra of D_2O and HDO molecules. Figure 3 shows the IR absorption spectra of beryl crystals grown in D_2O solutions. Here the IR absorption spectra in the stretching range are not a strict replica of the H_2O spectra with the band frequencies that are smaller by the predicted factor of about 1.35 (De Donato et al. 2004), because the growth solution also contained HDO molecules. We observe that the D_2O-related vibrational features are similar to those of H_2O molecules. There are two types of D_2O molecules whose IR absorbance bands are listed in Table 2. The intense bands observed at 2745 and 2631 cm^{-1} in the parallel polarization (**E**||*c*) and weak bands in the perpendicular polarization (**E**⊥*c*) at 2728 and 2635 cm^{-1} are related to type I and II D_2O molecules. The pair of bands located in the stretching range of OH (at 3655 and 3631 cm^{-1}) and OD (at 2687 and 2676 cm^{-1}) vibration frequencies are related to HDO molecules. For the

sample #3875 the bands at 3631 and 2676 cm^{-1} are observable as a shoulder on the background of more intense bands at 3655 and 2687 cm^{-1}. For the fundamental bands the full width at half-maximum (FWHM) is no more than 10 cm^{-1} besides the band at 2728 cm^{-1} (FWHM ~ 35 cm^{-1}) which is ascribed to the ν_3 mode of D_2O II molecule. There are weak bands in the region from 3700 to 3600 cm^{-1} attributed to the stretching bands of H_2O molecules. In the range of OD stretching vibrations of the synthetic beryl #3855 and Ural emerald very weak bands are also observable. In Figures 1c and 2c we see that **E**||*c* polarization is more favorable for the registration of OD absorption bands. For beryl #3855 three bands at 2741, 2687, and 2675 cm^{-1} were observed (Fig. 1c). For Ural emerald four bands at 2741, 2687, 2673 and 2641 cm^{-1} were observed (Fig. 2c).

DISCUSSION

Our main observations of the spectral features connected with the H_2O molecules are in agreement with the results of previous publications. In particular, for the type I H_2O molecule the position of the strong ν_3 band at 3700 cm^{-1} is not disputed whereas the weak ν_1 band has debated to occur at 3550 cm^{-1} (Wood and Nassau 1967) or from 3630 to 3606 cm^{-1} (Charoy et al. 1996; Łodzinsky et al. 2005). Taking into account that the difference between the ν_3 and ν_1 mode of the H_2O molecule is usually about 100 cm^{-1} and that in Raman spectra the ν_1 mode is observed at 3607 cm^{-1} (Kolesov and Geiger 2000; Łodzinsky et al. 2005), we also assign the band at 3606 cm^{-1} observed in our samples to the ν_1 mode of the type I H_2O molecule.

In contrast to the type I H_2O, the observed intensity of the ν_3 band of the type II H_2O molecule is lower than that of the ν_1 band. The ν_3 band of the type II H_2O molecule is located in the range of 3670-3650 cm^{-1} (Charoy et al. 1996; Lodzinsky et al. 2005; Wood and Nassau 1967) or can be observed even at 3643 cm^{-1} (Bellatreccia et al. 2008). For type II H_2O the position of

the strong ν_1 band is observed at frequencies ranging from 3600 to 3587 cm^{-1} (Bellatreccia et al. 2008; Charoy et al. 1996; Della Ventura et al. 2015; Fukuda and Shinoda 2009; Łodzinsky et al. 2005; Wood and Nassau 1967) and at 3597 cm^{-1} in Raman spectra (Kolesov and Geiger 2000; Łodzinsky et al. 2005). It is known that the anions have a significant effect on the hydroxyl stretching modes' frequencies because of hydrogen bonding (Cammarata et al. 2001; Masaki et al. 2010). It was found that the difference ν_3- ν_1 remains almost constant within the range 70-80 cm^{-1} for 2:1 complexes of water (Cammarata et al. 2001 and Refs therein). In contrast the cations such as alkali ions have a weak influence on the vibrations frequencies, however, in the Cs^+-H_2O complex a dramatic decrease in the ratio of the vibrational intensities of the asymmetric and symmetric OH stretches of water has been reported (Lisy 1997; Vaden et al. 2002). Also in beryl for type II water an inverse ratio between intensities of ν_3 and ν_1 bands is observed whereas this ratio for type I water is similar to that of free water molecule (i.e. the ν_3 band is stronger than the ν_1 band). Along with small differences relative to the free water stretching frequencies the theoretical shifts in the stretching frequencies are less than 20 cm^{-1} when Li^+ substitutes for Na^+ in their complexes with H_2O (Lee et al. 2004). Therefore, the small changes in the frequencies observed for type II H_2O in beryl in different studies might be associated with a weak influence of the different alkali ions. At this point it is difficult to establish the individual frequencies of IR absorbance bands for specific alkali ions besides sodium ion. It is now found that type II H_2O associated with Na occurs in channels of beryl in two configurations: "doubly coordinated" H_2O-Na^+-H_2O and "singly coordinated" Na^+-H_2O (Fukuda and Shinoda 2008; Della Ventura et al. 2015). The former configuration is characterized by the bands at 3660, 3600 and 1620 cm^{-1}, while the latter configuration is characterized by the bands at 3643, 3589 and 1633 cm^{-1}. The bands at 3643 and at 3587 cm^{-1} that were tentatively assigned to the Li^+-H_2O complex in the flux

grown beryl (Bellatreccia et al. 2008), possibly, are related to the Na^+-H_2O complex because the trace amounts of Na were also detected in this sample. In our synthetic beryl #3855 the doubly coordinated type II H_2O (because of the small ratio Li/H_2O, see Table 1) may be formed only with the Li^+ ion and the modes ν_3 at 3671 and ν_1 at 3599 cm^{-1} are observed (Fig. 1a). In our natural and synthetic beryls some discrepancies in the IR band positions especially for type II H_2O are observed. In Ural emerald the ν_3 band is located at 3660 cm^{-1}, because type II H_2O is coordinated with a Na^+ ion (in Table 1 a partial microprobe analysis of Ural emerald taken from work of Mashkovtsev and Smirnov 2005 is listed). Also the structural features of these two beryls are manifested in the frequencies of the libration mode and the $2\nu_2$ overtone (see Table 2).

By analogy with H_2O we conclude that the two pairs of ν_3 (at 2745 and 2728 cm^{-1}) and ν_1 modes (at 2635 and 2631 cm^{-1}) are related to type I and type II D_2O molecules, respectively (see Fig. 2a,c). In the HDO molecule the vibrations of OH and OD groups are independent. Therefore in the range of stretching frequencies the IR absorption spectra of the HDO molecule include OH (at 3655 and 3631 cm^{-1}) and OD (at 2687 and 2676 cm^{-1}) vibration bands which are about half way between the frequencies of the ν_1 and ν_3 modes of H_2O and D_2O, respectively (see Fig.2a,c and Table 2). In the higher-frequency range weak and very weak lines belong to transitions involving multiple excitations (Fig. 2b,d and Table 2). We cannot observe the bending modes of the D_2O and HDO molecules because of a considerable overlap with lattice vibrations. We use the frequencies of about 1200 and 1400 cm^{-1} for the bending modes of D_2O and HDO (cf. Halonen and Carrington 1988; Wang et al. 2004) to ascribe the overtone manifolds (Table 2). Following the D_2O designation there are HDO molecules of types I and II with the frequencies of OH and OD stretching vibrations for HDO II somewhat lower in comparison with that of HDO of type I. As might be expected, the absorbance bands related to the libration modes are observed

for the D_2O molecule. A satellite at 2876 cm^{-1} with a separation of approximately 130 cm^{-1} from the D_2O I ν_3 mode is well distinguished for the **E**$\perp c$ polarization. Its low-frequency counterpart is overlapped with the D_2O I ν_1 band and is poorly resolved. For D_2O II the position of the combination band related to the libration mode is slightly different for two samples as in the case of H_2O II (Table 2). We determine the libration modes with frequencies of about 230 and 290 cm^{-1} as the frequency differences between the satellites around 2956 and 3016 cm^{-1} and ν_3 fundamental band at 2728 cm^{-1} for the samples #3875 and #3871, respectively.

Now we can explain very weak bands observed in the range of OD stretching vibrations for the sample #3855 and Ural emerald with the natural isotopic abundance of deuterated water (Figures 1c and 2c). For these samples the frequencies of OD stretching vibrations agree closely with those shown in Figure 3 and Table 2 for the samples #3875 and #3871 but the concentration ratio of HDO and D_2O differs markedly. For Ural emerald the amplitudes of the bands related to HDO and D_2O molecules are comparable. For the sample #3855 the band related to the ν_1 mode D_2O II is not observed at all. Furthermore for the sample #3855 and Ural emerald the band with maximum at 2741 cm^{-1} is relatively broad (FWHM ~ 70 cm^{-1} and FWHM ~ 60 cm^{-1}, respectively). It is difficult to explain taking into account that the widths of other bands at 2687 (FWHM = 7 cm^{-1}) and 2675 cm^{-1} (FWHM ~ 10 cm^{-1}) are comparable with those observed in the range of OD stretching vibrations of our D_2O-bearing synthetic samples. Hence for the sample #3855 the assignment of the broad band at 2741 cm^{-1} to the ν_3 mode of D_2O I molecules is questionable and a contribution of lattice vibration must be checked. Possibly distilled water used for beryl synthesis contains only HDO molecules in the negligible amounts.

To compare our data with the results of the previous work (De Donato et al. 2004) we also measured an unpolarized spectrum for the samples #3871 and #3875 (Fig. 3a,c). In

comparison with the polarized spectra all the fundamental bands do not change their positions except that the broad band around 2735 cm^{-1} (FWHM = 45 cm^{-1}) in the unpolarized spectrum apparently arises from the superimposition of two distinct bands at 2745 and 2728 cm^{-1} and, therefore, the position of the combined maximum is dependent on the relative quantities of D_2O I and D_2O II. (Fig. 3a,c). In the range between 2800 and 2600 cm^{-1}, the positions of the bands in our synthetic beryls are in good agreement with those observed by De Donato et al. (2004) in natural samples. Again our attention is focused on the broad width of the band around 3735 cm^{-1} (FWHM = 50 cm^{-1}) observed for the natural beryls (De Donato et al. 2004). Such a width cannot be explained only by the superimposition of two bands related to the ν_3 mode of D_2O I and D_2O II because the substantial contribution of the former band is under question and the latter is very weak in comparison to the ν_1 band of D_2O II. Another salient feature is that the relative intensities of the bands are substantially dependent on the specific samples. We note that the band at 2816 cm^{-1} observed in Colombian emerald (De Donato et al. 2004) is probably related to the HCl molecule (Mashkovtsev and Solntsev 2002; Mashkovtsev and Smirnov 2004).

IMPLICATIONS

In summary, this study demonstrates that the uptake of D_2O and HDO molecules by the structural channels during synthesis of beryl in deuterated water is comparable with the content of H_2O molecules in natural beryl. As a result the frequencies of absorbance bands in the range of the stretching vibrations and their overtones and combination modes for D_2O and HDO molecules in the structural channels of beryl have been assigned. Our findings allow us to explain the IR absorbance bands in the range of OD stretching vibrations of natural beryl. This fact can play an important role in defining the speciation of deuterated water molecules in the

structural channels of beryl formed under different natural environments. Our results can apply to gemological practice because of an obvious distinction of isotopic content of distilled water used for the synthesis of emerald and water incorporated into the natural beryl. This distinction will be reflected in the FTIR spectra measured for synthetic and natural emeralds in the range of OD stretching vibrations.

We believe that presented results will be useful for better understanding the internal dynamics and energetics of various molecules that are localized within nano-sized cavities and are weakly coupled to the walls. Clearly, of particular interest is the water molecule because of importance of its properties (physical, chemical, biological, etc.) when confined to nano-pores that are found on the Earth in various natural and synthetic frameworks, like zeolites, clays, silica gels, biological systems, carbon nanotubes, fullerenes, molecular clusters, etc.

ACKNOWLEDGMENTS

We thank Ian Swainson and three reviewers for their fruitful comments. The authors would like to thank O.A. Kozmenko for chemical analyses and I.N. Kupriyanov for FTIR spectra measurements. The synthesis of beryl crystals was carried out on the equipment, kindly provided by the firm TAIRUS (Novosibirsk, Russia). The research was supported by the Russian Foundation for Basic Research (Grant 14-02-00255) and by the Russian Ministry of Education and Science (Program “5top100”).

REFERENCES CITED

Adamo, I., Gatta, G.D., Rotiroti, N., Della, V., and Pavese, A. (2008) Gemmological investigation of a synthetic blue beryl: a multi-methological study. Mineralogical

Magazine, 72, 799-808.

Aines, R.D., and Rossman, G.R. (1984) The high temperature behavior of water and carbon dioxide in cordierite and beryl. American Mineralogist, 69, 319-327.

Aurisicchio, A., Grubessi, O., and Zecchini, P. (1994) Infrared spectroscopy and crystal chemistry of the beryl group. Canadian Mineralogist, 32, 55-68.

Bellatreccia, F., Della Ventura, G., Piccinini, M., and Grubessi, O. (2008) Single-crystal polarized-light FTIR study of an historical synthetic water-poor emerald. Neues Jahrbuch für Mineralogie - Abhandlungen, 185, 11-16.

Cammarata, L., Kazarian, S.G., Salter, P.A., and Welton, T. (2001) Molecular states of water in room temperature ionic liquids. Physical Chemistry Chemical Physics, 3, 5192-5200.

Charoy, B., De Donato, P., Barres, O., and Pinto-Coelho, C. (1996) Channel occupancy in an alkali-poor beryl from Serra Branca (Goias, Brazil): Spectroscopic characterization. American Mineralogist, 81, 395-403.

Damon, P.E., and Kulp, J.L. (1958) Excess helium and argon in beryl and other minerals. American Mineralogist, 43, 433-459.

De Donato, P., Cheiletz, A., Barres, O., and Yvon, J. (2004) Infrared spectroscopy of OD vibrators in minerals at natural dilution: Hydroxyl groups in talc and kaolinite, and structural water in beryl and emerald. Journal of Applied Spectroscopy, 58, 521-527.

Della Ventura, G., Bellatreccia, F., Rossi, P. (2007) The single-crystal, polarized-light, FTIR spectrum of stoppaniite, the Fe analogue of beryl. Physics and Chemistry of Minerals, 34, 727-731.

Della Ventura, G., Radica, F., Bellatreccia, F., Freda, C., Cestelli Guidi, M. (2015) Speciation and diffusion profiles of H_2O in water-poor beryl: comparison with cordierite. Physics and Chemistry of Minerals (in press).

Fukuda, J., and Shinoda, K. (2008) Coordination of water molecules with Na^+ cations in a beryl channel as determined by polarized IR spectroscopy. Physics and Chemistry of Minerals, 35, 347-357.

Gorshunov, B.P., Zhukova, E.S. Torgashev, V.I., Lebedev, V.V., Shakurov, G.S., Kremer, R.K., Pestrjakov, E.V., Thomas, V.G., Fursenko, D.A., Prokhorov, A.S., and Dressel, M. (2013) Quantum behavior of water molecules confined to nanocavities in gemstones. Journal of Physical Chemistry Letters, 4, 2015-2020.

Halonen, L., and Carrington, T. (1988) Fermi resonances and local modes in water, hydrogen sulfide, and hydrogen selenide. Journal of Chemical Physics, 88, 4171-4185.

Kolesov, B.A., and Geiger, C.A. (2000) The orientation and vibrational states of H_2O in synthetic alkali-free beryl. Physics and Chemistry of Minerals, 27, 557-564.

Lee, H.M., Tarakeshwar, P., Parl, J., Kolaski, M.R., Yoon, Y.J., Yi Hai-Bo, Kim, W.Y., and Kim, K.S. (2004) Insights into the structure, energetic, and vibrations of monovalent cation-(water)1-6 clusters. Journal of Physical Chemistry A, 108, 2949-2958.

Lisy, J.M. (1997) Spectroscopy and structure of solvated alkli-metal ions. International Reviews in Physical Chemistry, 16, 267-289.

Łodziński, M., Sitarz, M., Stec, K., Kozanecki, M., Fojud, Z., and Jurga, S. (2005) ICP, IR, Raman, NMR investigations of beryls from pegmatites of the Sudety Mts. Journal of Molecular Structure, 744-747, 1005-1015.

Makreski, P., and Jovanvski, G. (2009) Minerals from Macedonia XXIII. Spectroscopic and

structural characterization of schorl and beryl cyclosilicates. Spectrochimica Acta Part A: Molecular Spectroscopy, 73, 460-467.

Manier-Glavinaz, V., Couty, R., and Lagache, M. (1989) The removal of alkalis from beryl: Structural adjustments. Canadian Mineralogist, 27, 663-671.

Masaki, T., Nishikawa, K., and Shirota, H. (2010) Microscopic study of ionic liquid-H_2O systems: Alkyl-group dependence of 1-alkyl-3-methylimidazolium cation. Journal of Physical Chemistry B, 114, 6323−6331.

Mashkovtsev, R.I. and Solntsev, V.P. (2002) Channel constituents in synthetic beryl: ammonium Physics and Chemistry of Minerals, 29, 65-71.

Mashkovtsev, R.I., and Smirnov, S.Z. (2004) The nature of channel constituents in hydrothermal synthetic emerald. Journal of Gemmology, 29, 215-227.

Mashkovtsev, R.I., and Thomas, V.G. (2005) Nitrogen atoms encased in cavities within the beryl structure as candidates for cubits. Applied Magnetic Resonance, 28, 401-409.

Sherriff, B.L., Grundy, H.D., Hartman, J.F., Hawthorne, F.C., and Černý, P. (1991) The incorporation of alkalis in beryl: multi-nuclear MAS NMR and crystal-structure study. Canadian Mineralogist, 29, 271-285.

Thomas, V. G., and Klyakhin, V. A. (1987) The specific features of beryl doping by chromium under hydrothermal conditions. In N. V. Sobolev, Ed., Mineral Forming in Endogenic Processes, p. 60–67. Nauka, Novosibirsk (in Russian).

Vaden, T.D., Forinash, B., and Lisy, J.M. (2002) Rotational structure in the asymmetric OH stretch of $Cs^+(H_2O)Ar$. Journal of Chemical Physics, 117, 4628-4631.

Wahler, W. (1956) Über die Kristallen eingeschlossenen Flussigkeiten und Gase. Geochimica et Cosmochimica Acta, 9, 105-135.

Wang, Z., Pakoulev, A., Pang, Y., and Dlott, D.D. (2004) Vibrational substructure in the OH stretching transition of water and HOD. Journal of Physical Chemistry, 108, 9054-9063.

Wood, D.L., and Nassau, K. (1967) Infrared spectra of foreign molecules in beryl. Journal of Chemical Physics, 47, 2220-2228.

Zhukova, E.S. Torgashev, V.I., Gorshunov, B.P., Lebedev, V.V., Shakurov, G.S., Kremer, R.K., Pestrjakov, E.V., Thomas, V.G., Fursenko, D.A., Prokhorov, and A.S., Dressel, M. (2014) Vibrational states of a water molecule in a nano-cavity of beryl crystal lattice. Journal of Chemical Physics, 140, 224317.

Zimmerman, J.L., Giuliani, G., Cheiletz, A., and Arboleda, C. (1997) Mineralogical significance of fluids in channels of Colombian emeralds: a mass-spectrometric study. International Geology Review, 39, 425-437.

Zwaan, J.C., Jacob, D.E., Häger, T., Neto, M.T.O.C., and Kanis, J. (2012) Emeralds from the Fazenda region, rio grande do norte, Brazil. Gems and Gemology, 48, 2-17.

Figure captions

Fig. 1. Polarized IR absorption spectra of H_2O and HDO molecules in the structure of synthetic beryl #3855: (a) the fundamental range, (b) the range of overtones and combination bands, and (c) the range of OD stretching vibrations. The thickness of the plates is indicated.

Fig. 2. Polarized IR absorption spectra of H_2O, D_2O and HDO molecules in the structure of natural emerald from Urals: (a) the fundamental range, (b) the range of overtones and combination bands, and (c) the range of OD stretching vibrations. The thickness of the plates is indicated.

Fig. 3. Polarized IR absorption spectra of D_2O and HDO molecules in the structure of synthetic beryl crystals #3871 and #3875: (a) and (c) the fundamental range, (b) and (d) the range of overtones and combination bands. The thickness of the plates is indicated.

Table 1. Chemical analyses (wt %) and structural formulae (18O basis) of synthetic beryls and partial microprobe analysis of Ural emerald (Mashkovtsev and Smirnov 2004)

Sample No.	SiO_2	Al_2O_3	BeO	Fe_2O_3	Cr_2O_3	CuO	Li_2O	Na_2O	LOI (H_2O +D_2O)	Total
3855	66.42	18.60	13.42	0.02	0.00	0.03	0.27	0.01	1.34	100.10
3871	66.29	18.59	13.35	0.04	0.00	0.02	0.30	0.01	1.66	100.25
3875	65.88	18.70	13.72	0.06	0.36	0.03	0.06	0.00	0.99	99.80
Ural	64.86	16.89	nd	0.28	0.17	-	nd	0.82	nd	84.32
		Formula								
3855	$(Be_{2.922}Si_{0.01}Cu_{0.002}Li_{0.066})_3(Al_{1.987}Si_{0.012}Fe_{0.001})_2Si_6O_{18}(Na_{0.001}Li_{0.032})_{0.033}(H_2O)_{0.4}$									
3871	$(Be_{2.912}Si_{0.014}Cu_{0.002}Li_{0.073})_3(Al_{1.99}Si_{0.008}Fe_{0.002})_2\ Si_6O_{18}(Na_{0.001}Li_{0.037})_{0.038}(D_2O,H_2O)_{0.5}$									
3875	$(Be_{2.989}Si_{0.006}Cu_{0.002}Li_{0.003})_3(Al_{1.97}Fe_{0.004}Cr_{0.026})_2(Si_{5.971}Al_{0.029})_6O_{18}(Na_{0.001}Li_{0.019})_{0.02}(D_2O,H_2O)_{0.3}$									

LOI – loss on ignition, nd – not determined

352

Table 2. IR peak locations (cm^{-1}) for absorption bands of H_2O, HDO, and D_2O molecules in beryl

H_2O				D_2O, HDO			
Natural emerald, Ural	Synthetic beryl # 3855	Polarization relative to *c*-axis	Assignment*	Synthetic beryl # 3871	Synthetic emerald # 3875	Polarization relative to *c*-axis	Assignment
7143	7144	∥	H_2O I: $\nu_1 + \nu_3$	7144	7144	∥	HDO I: 2νOH
5276	5276	∥	H_2O I: $\nu_2 + \nu_3$	5297	5297	∥	D_2O I: $\nu_1 + \nu_3$
3979	4057	∥	H_2O II: ν_3+νlibr	5038	5038	∥	HDO I: δ + νOH
3850	3863	⊥	H_2O I: ν_3+νlibr	4076	4076	∥	HDO I: δ + νOD
3697	3700	∥	H_2O I: ν_3	3914	3914	∥	D_2O I: $\nu_2 + \nu_3$
3660	3671	⊥	H_2O II: ν_3	3700	3700	∥	H_2O I: ν_3
3606	3606	⊥	H_2O I: ν_1	3655	3655	∥	HDO I: νOH
3598	3599	∥	H_2O II: ν_1	3636		∥	HDO II: νOH
3236	3222	∥	H_2O II: $2\nu_2$	3601	3601	∥	H_2O II: ν_1
2687	2687	∥	HDO I: νOD	3019	2956	∥	D_2O II: ν_3+νlibr
2673	2675	∥	HDO II: νOD	2876	2876	⊥	D_2O I: ν_3+νlibr
2641		∥	D_2O II: ν_1	2745	2745	∥	D_2O I: ν_3
2360		⊥	CO_2	2728	2729	⊥	D_2O II: ν_3
1633	1631	∥	H_2O II: ν_2	2687	2687	∥	HDO I: νOD
1600	1599	⊥	H_2O I: ν_2	2676	2676sh	∥	HDO II: νOD
				2635	2635	⊥	D_2O I: ν_1
				2631	2634	∥	D_2O II: ν_1

353 *the assignment of H_2O and CO_2 IR absorption bands is attributed to Wood and Nassau (1967)

354

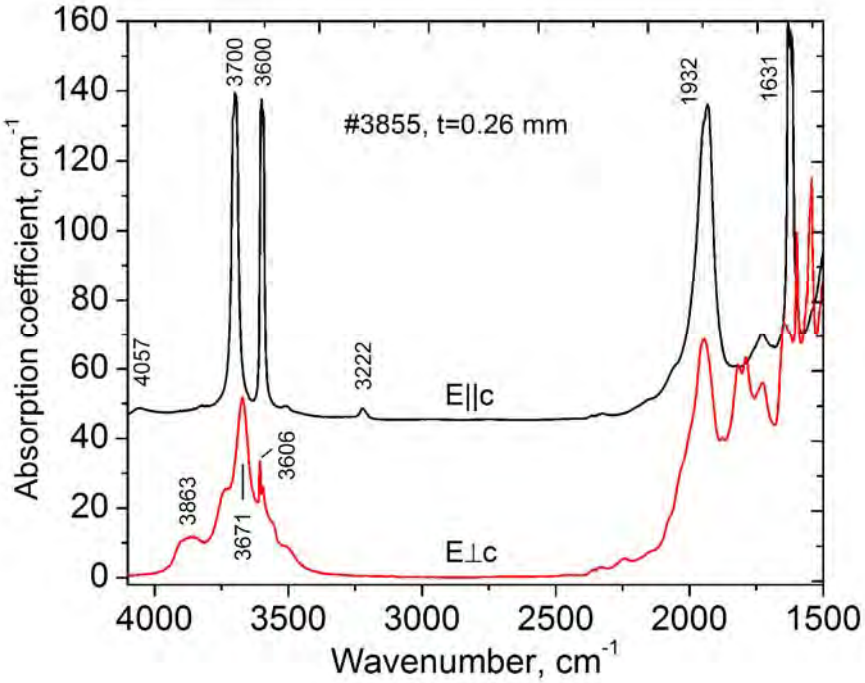
#3855, t=0.26 mm
3700
3600
1932
1631
4057
3222
E||c
3606
3863
3671
E⊥c
Absorption coefficient, cm-1
Wavenumber, cm-1

355 (a)

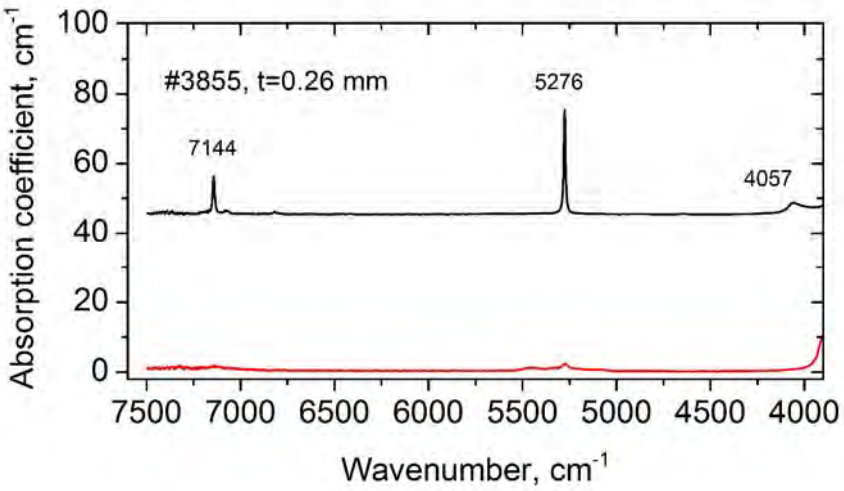
#3855, t=0.26 mm
5276
7144
4057
Absorption coefficient, cm-1
Wavenumber, cm-1

356 (b)

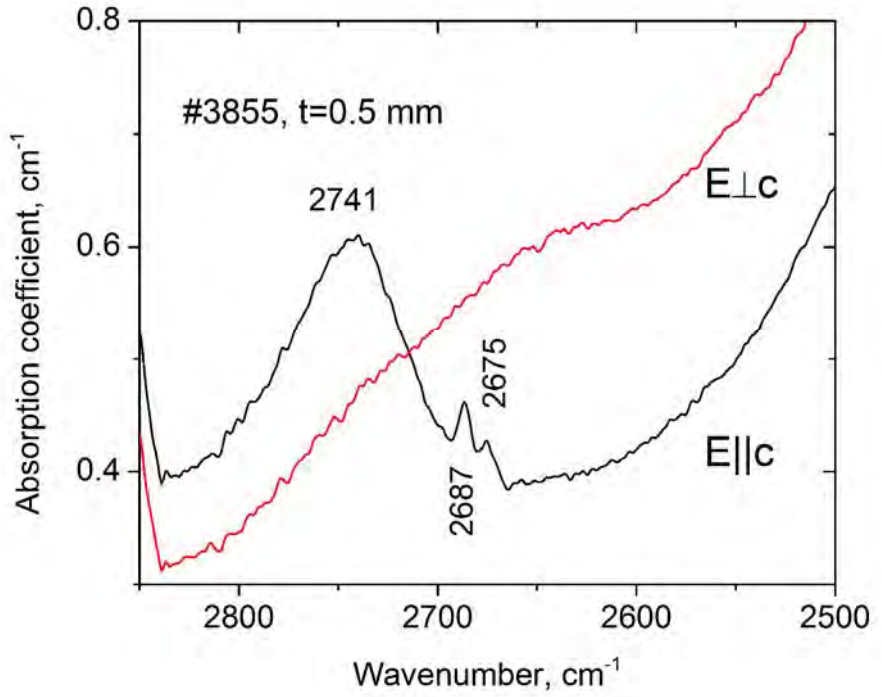

357 (c)

358 **Fig. 1.**

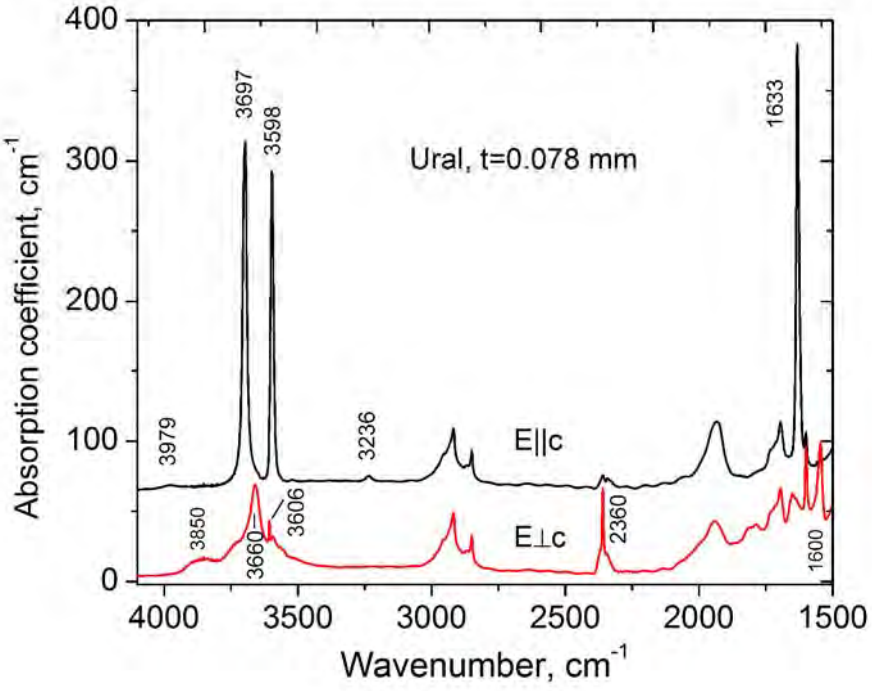

359 (a)

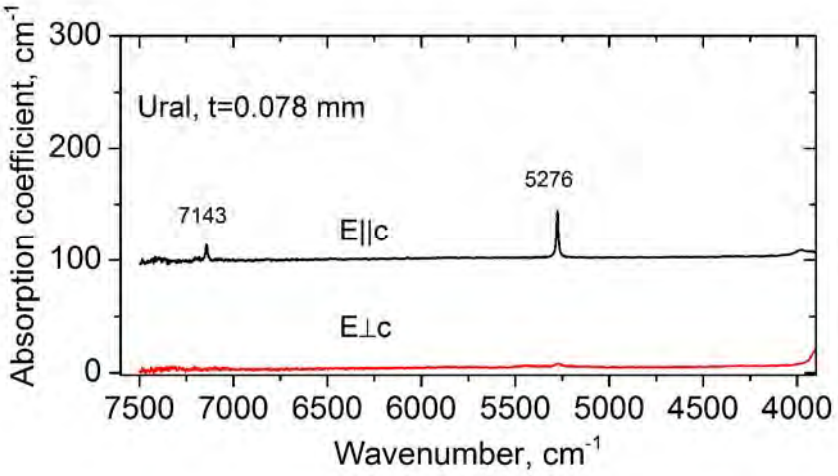

360 (b)

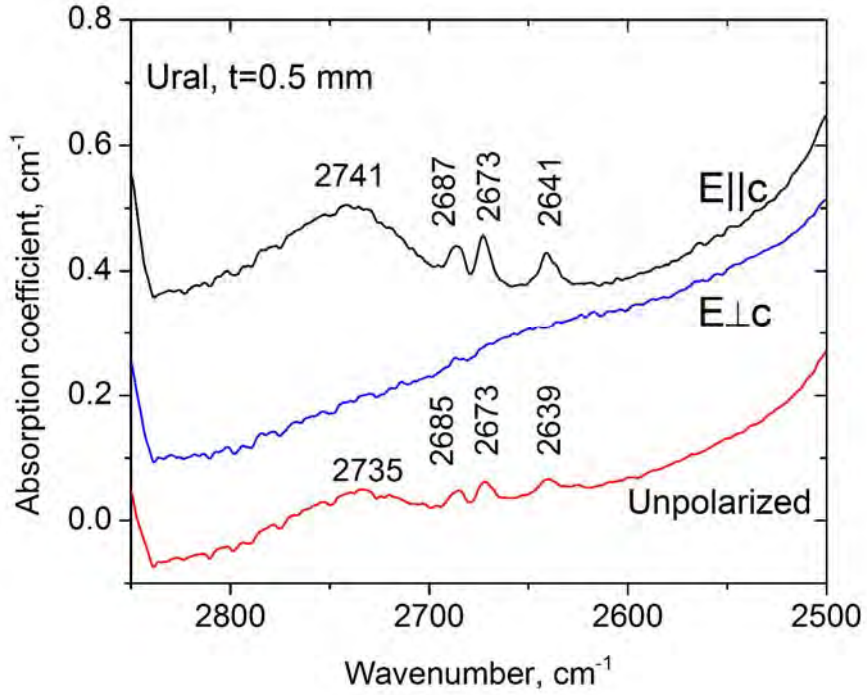

361 (c)

362 **Fig. 2**.

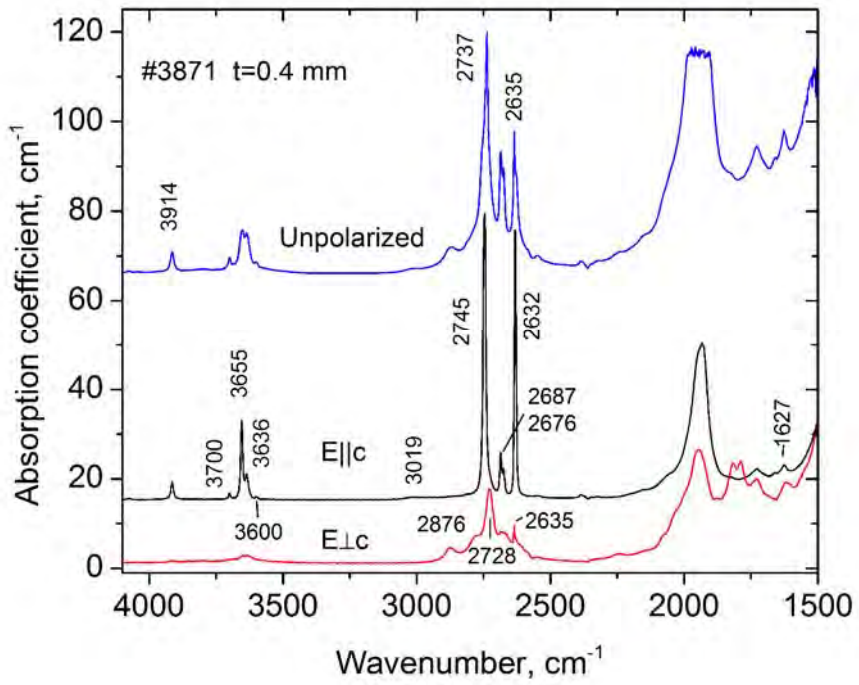
#3871 t=0.4 mm
Unpolarized
E||c
E⊥c
3914
3700
3655
3636
3600
3019
2737
2745
2635
2632
2687
2676
2876
2728
2635
1627
Absorption coefficient, cm-1
Wavenumber, cm-1

363 (a)

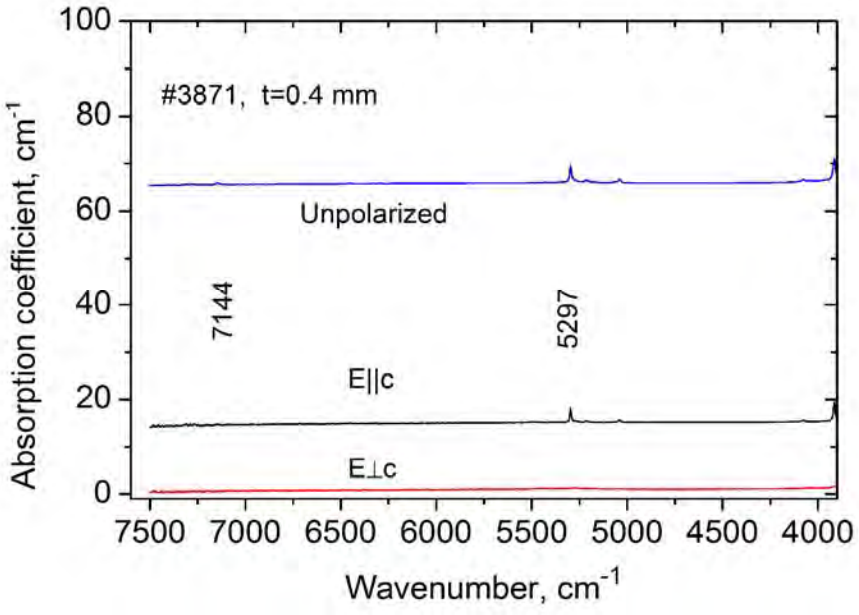
#3871, t=0.4 mm
Unpolarized
E||c
E⊥c
7144
5297
Absorption coefficient, cm-1
Wavenumber, cm-1

364 (b)

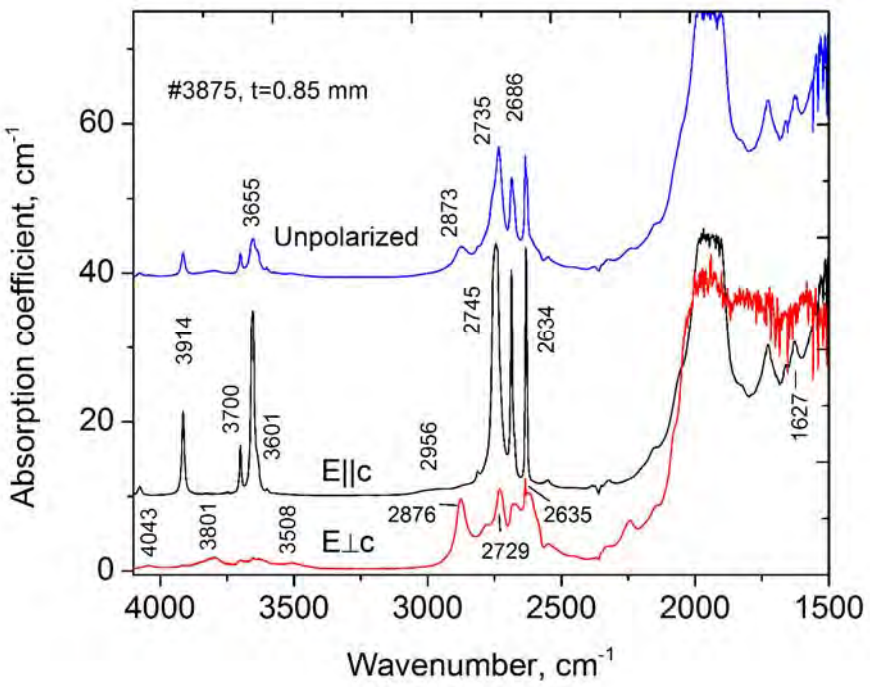

365 (c)

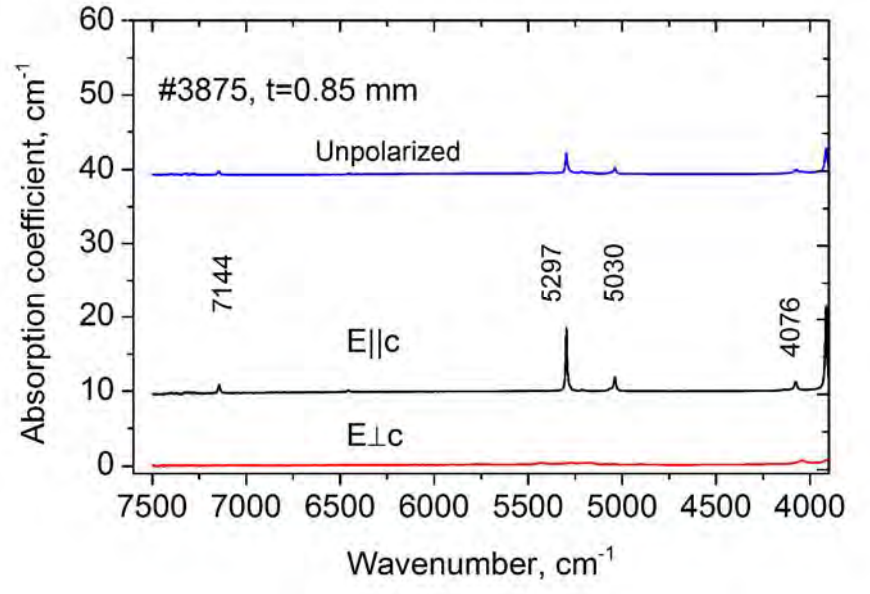

366 (d)

367 **Fig. 3.**

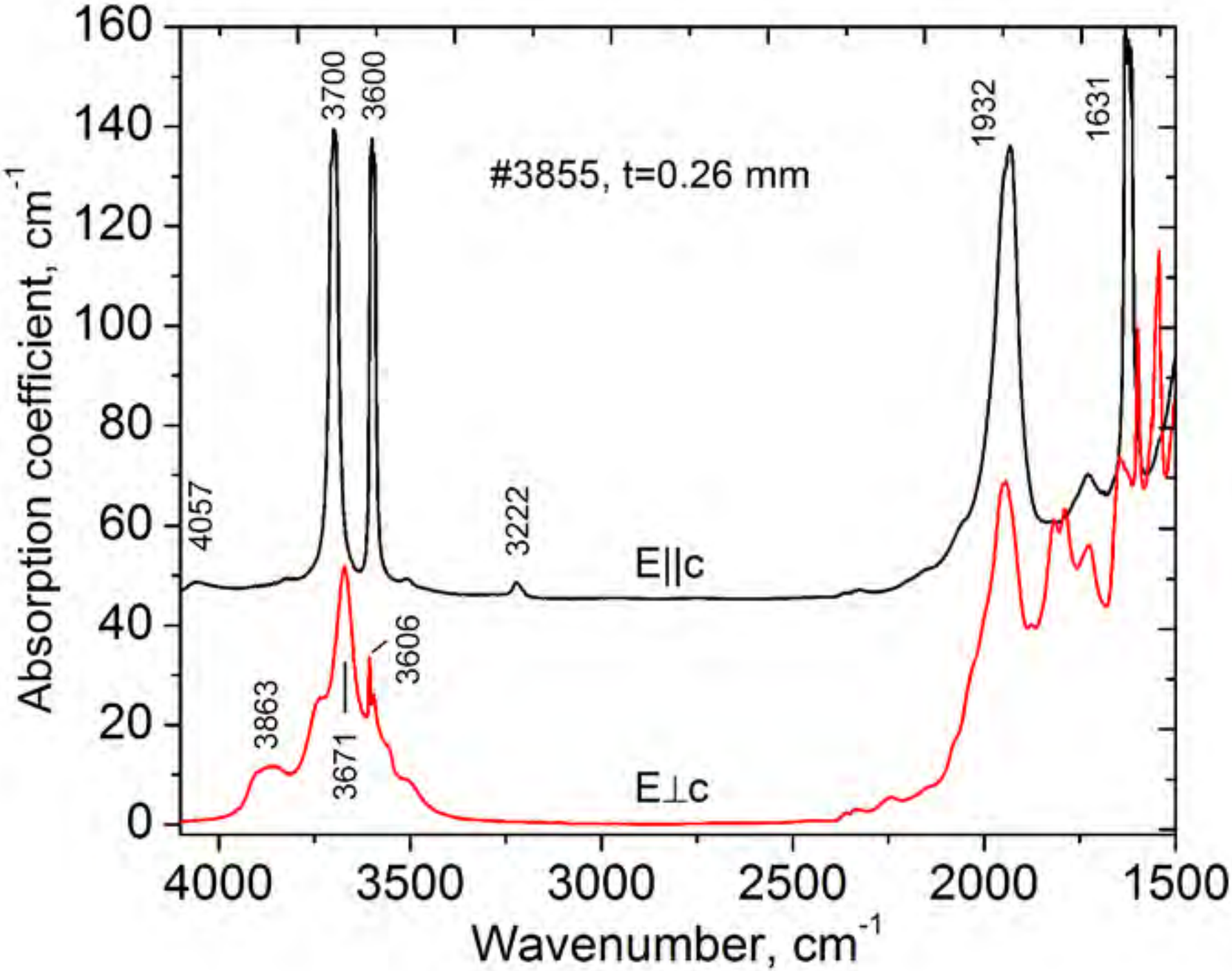
Absorption coefficient, cm-1
Wavenumber, cm-1
#3855, t=0.26 mm
E||c
E⊥c
4057
3700
3600
3222
1932
1631
3863
3671
3606
160
140
120
100
80
60
40
20
0
4000
3500
3000
2500
2000
1500

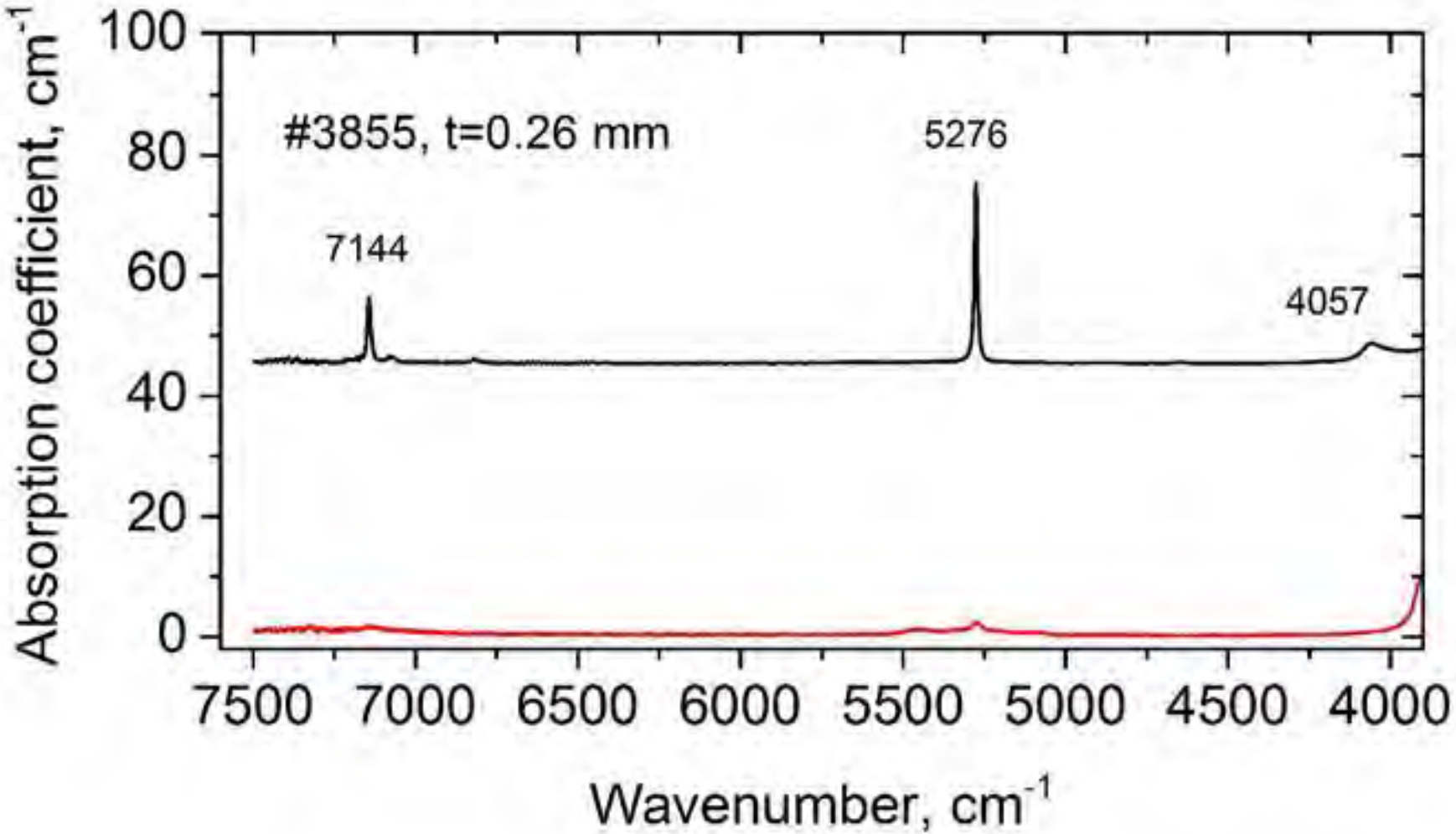
#3855, t=0.26 mm
5276
7144
4057
Absorption coefficient, cm-1
Wavenumber, cm-1
100
80
60
40
20
0
7500
7000
6500
6000
5500
5000
4500
4000

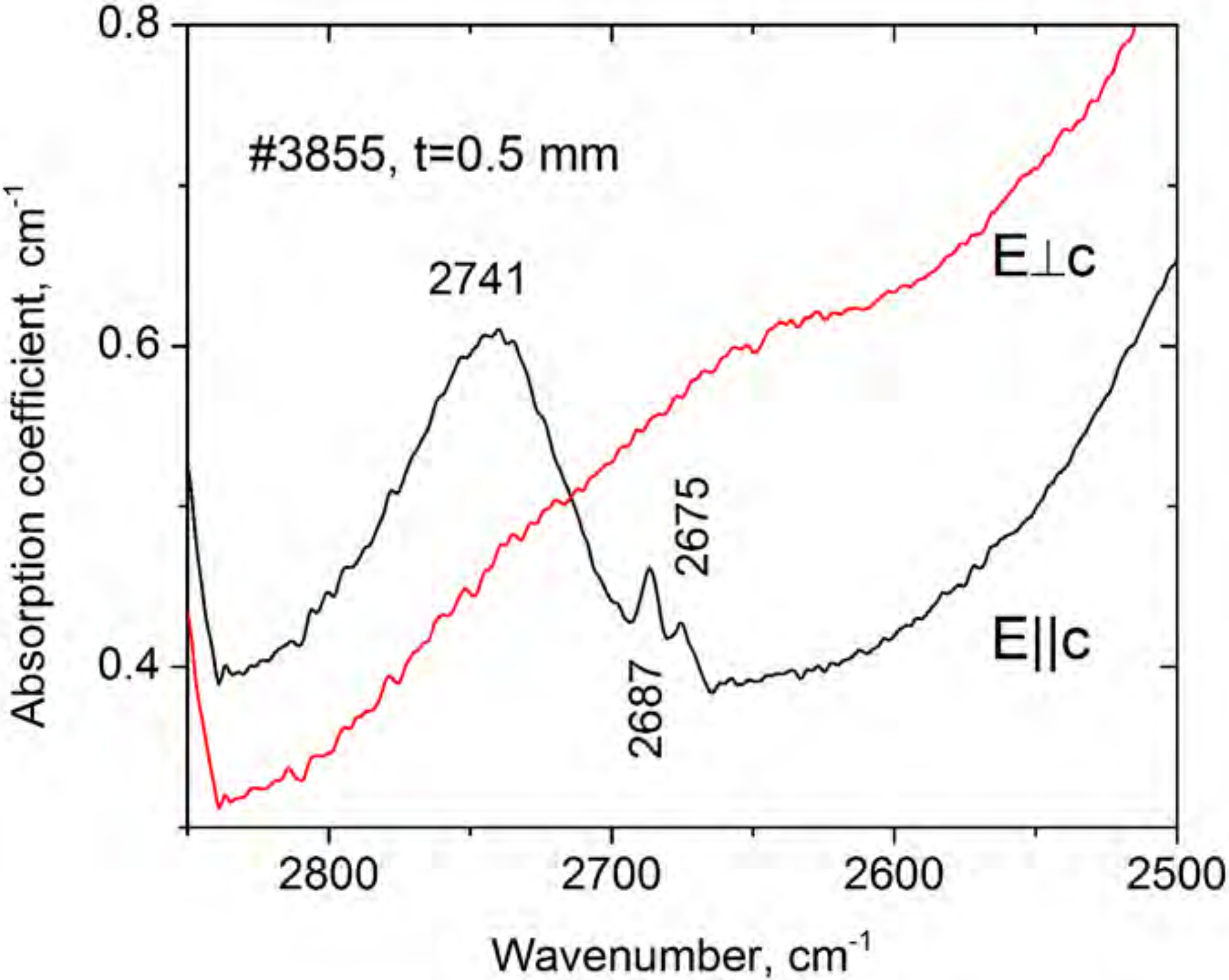
#3855, t=0.5 mm
2741
2675
2687
E⊥c
E||c
0.8
0.6
0.4
2800
2700
2600
2500
Absorption coefficient, cm-1
Wavenumber, cm-1

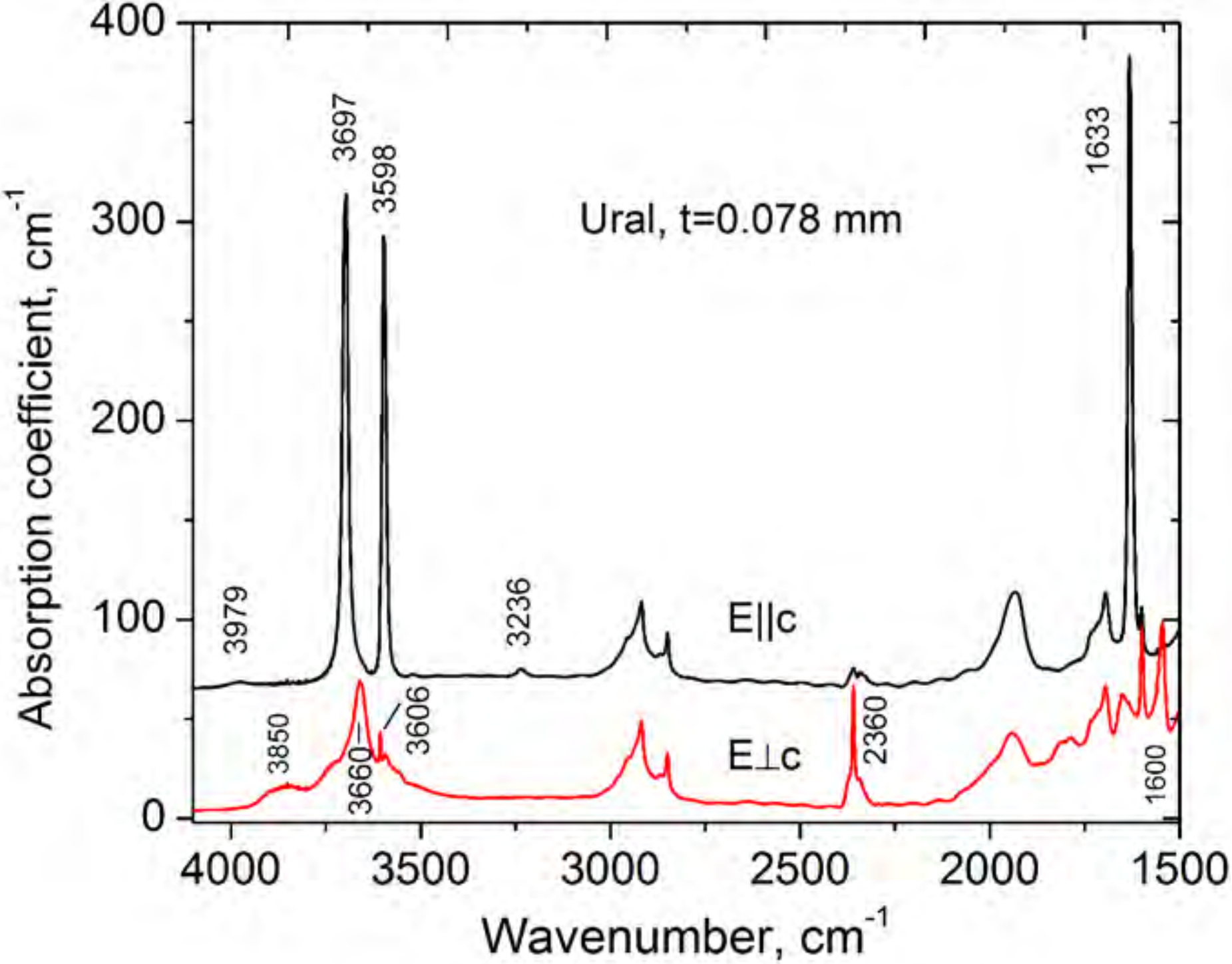
Absorption coefficient, cm-1
Wavenumber, cm-1
Ural, t=0.078 mm
E||c
E⊥c
3979
3697
3598
3236
1633
3850
3660
3606
2360
1600
400
300
200
100
0
4000
3500
3000
2500
2000
1500

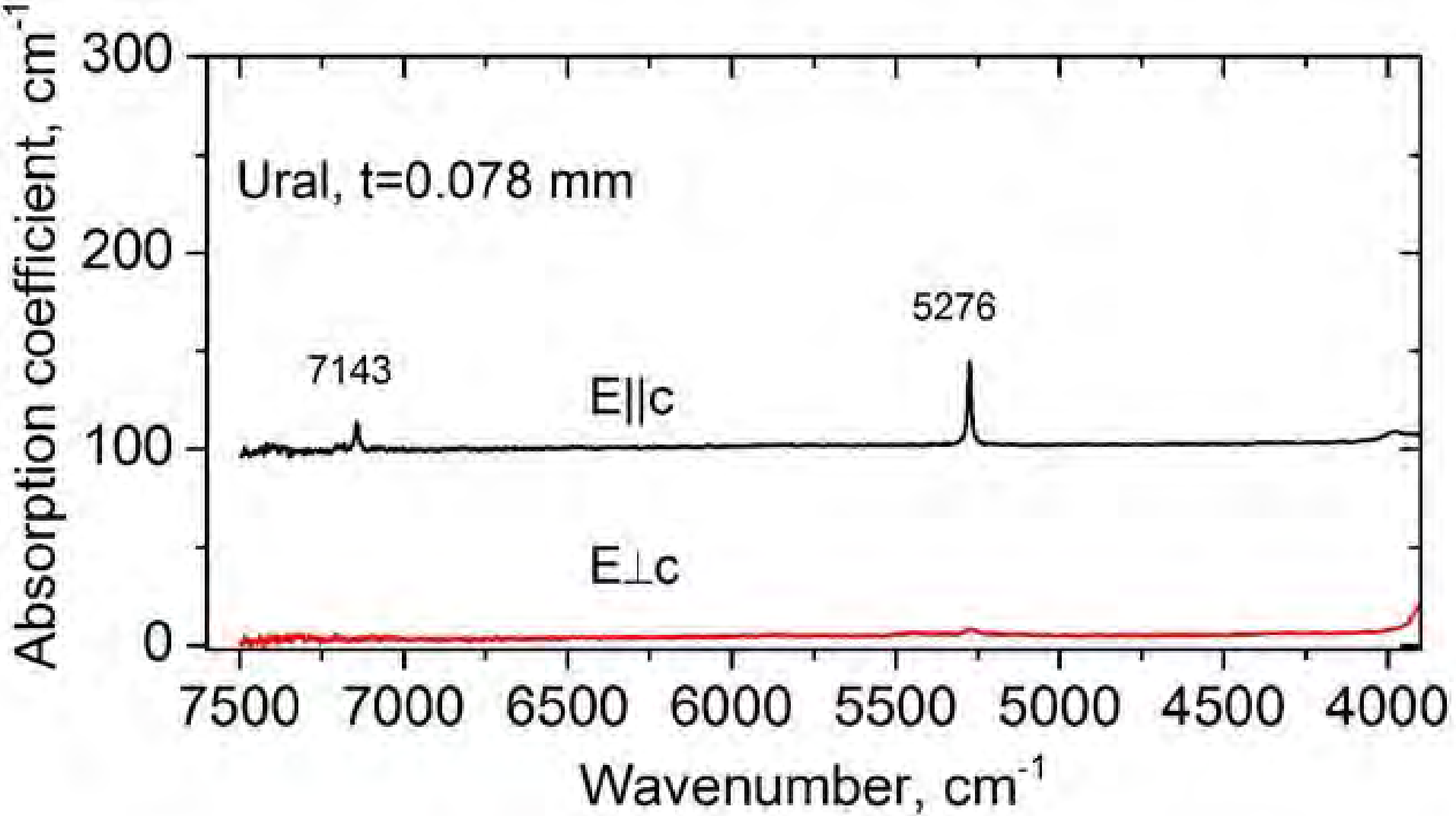
Absorption coefficient, cm-1
300
200
100
0
Ural, t=0.078 mm
5276
7143
E||c
E⊥c
7500
7000
6500
6000
5500
5000
4500
4000
Wavenumber, cm-1

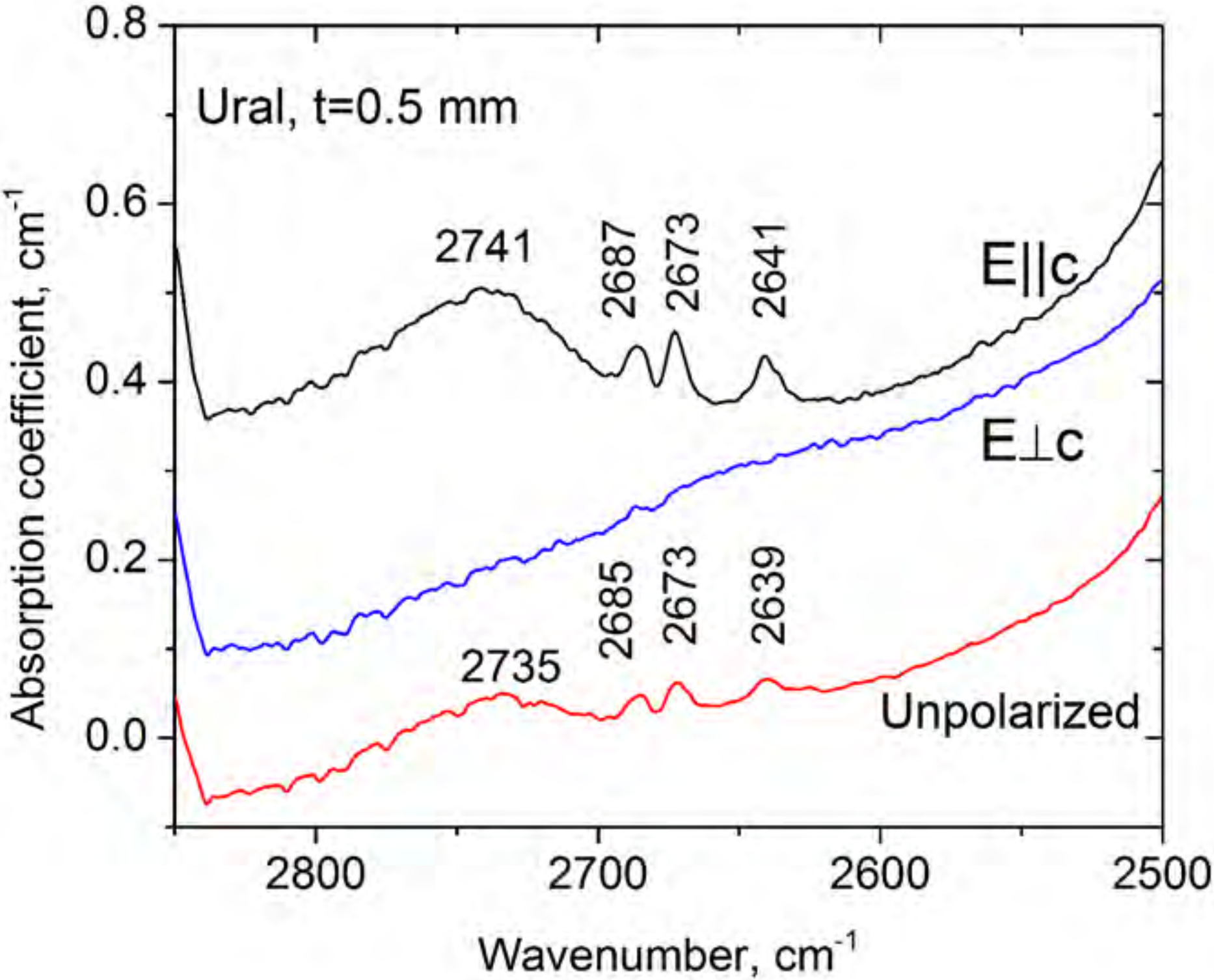
Ural, t=0.5 mm
2741
2687
2673
2641
E||c
E⊥c
2685
2673
2639
2735
Unpolarized
0.8
0.6
0.4
0.2
0.0
2800
2700
2600
2500
Absorption coefficient, cm-1
Wavenumber, cm-1

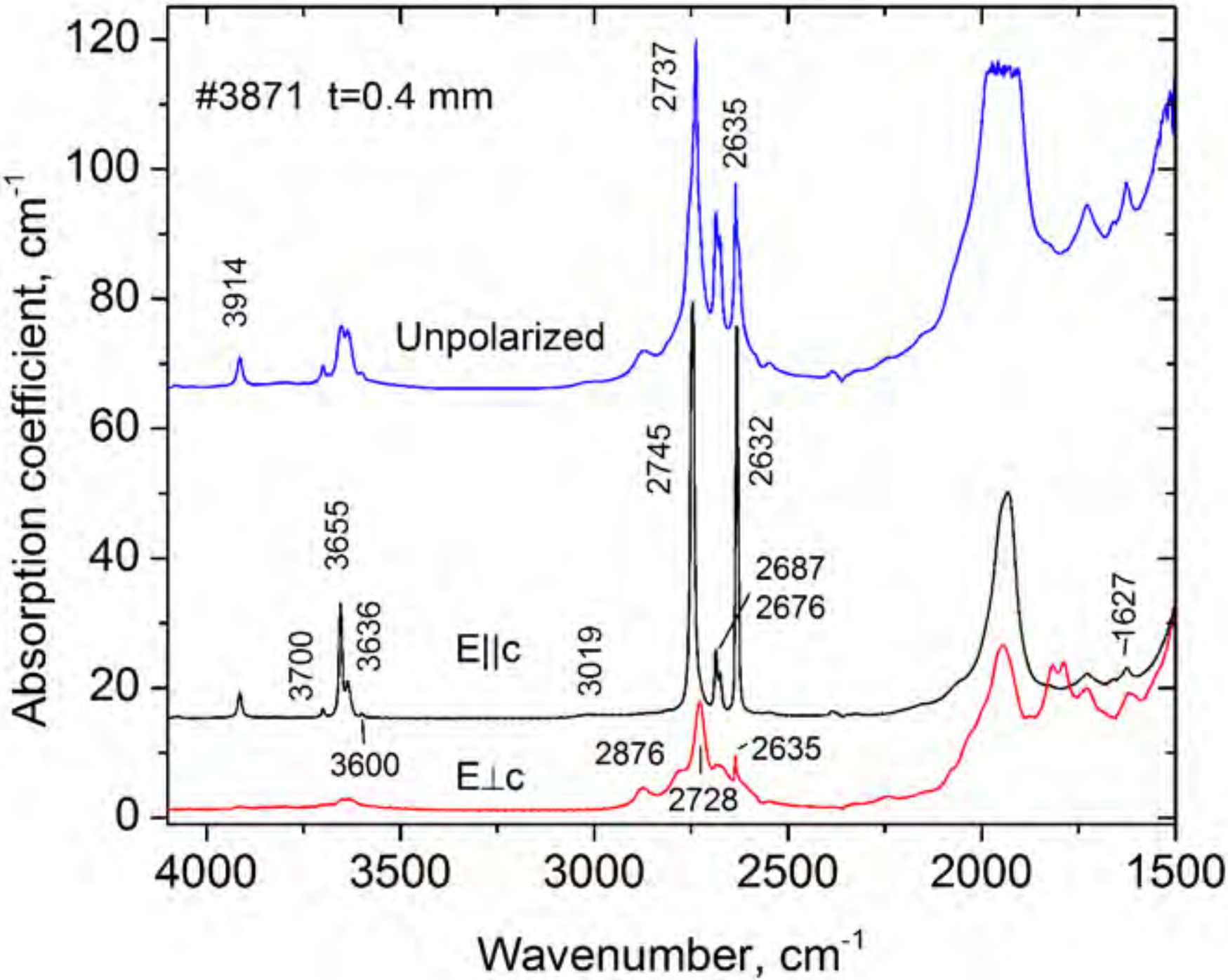
#3871 t=0.4 mm
Unpolarized
E||c
E⊥c
3914
2737
2635
2745
2632
3655
3700
3636
3600
3019
2687
2676
1627
2876
2728
2635
Absorption coefficient, cm-1
Wavenumber, cm-1
120
100
80
60
40
20
0
4000
3500
3000
2500
2000
1500

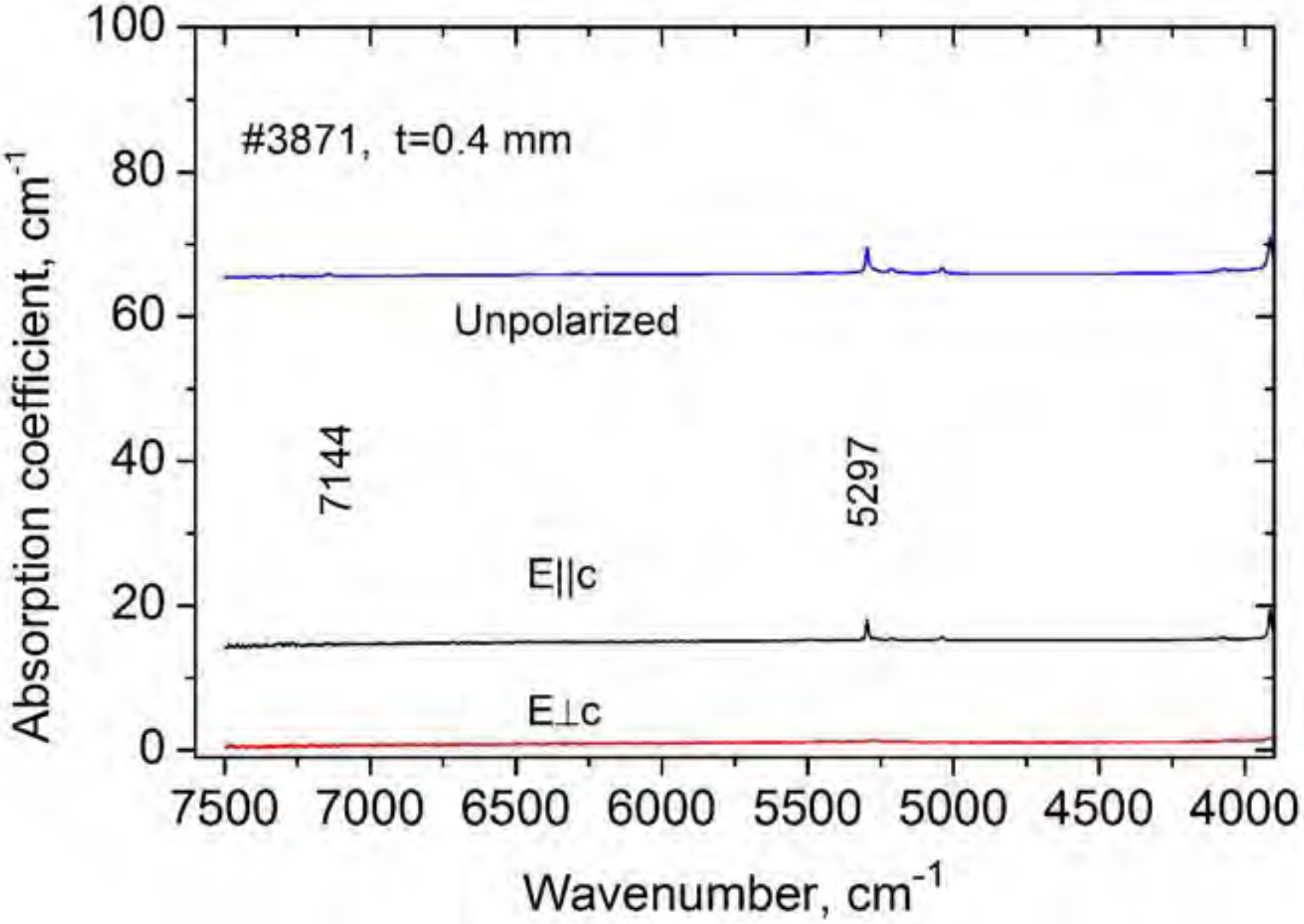
#3871, t=0.4 mm
Unpolarized
E||c
E⊥c
7144
5297
Absorption coefficient, cm-1
Wavenumber, cm-1
100
80
60
40
20
0
7500
7000
6500
6000
5500
5000
4500
4000

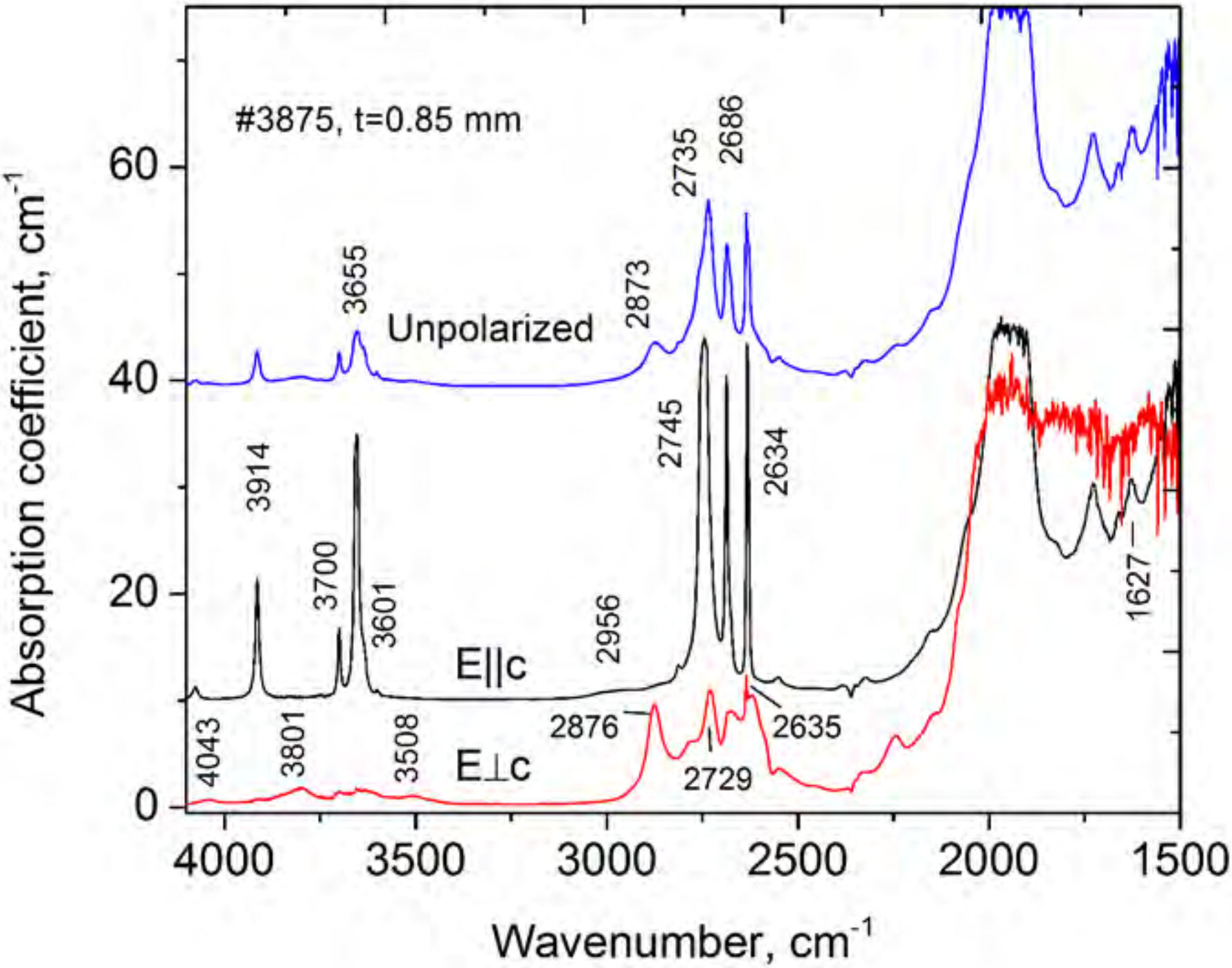
#3875, t=0.85 mm
Unpolarized
E||c
E⊥c
Absorption coefficient, cm-1
Wavenumber, cm-1
0
20
40
60
4000
3500
3000
2500
2000
1500
4043
3914
3801
3700
3655
3601
3508
2956
2876
2873
2745
2735
2729
2686
2635
2634
1627

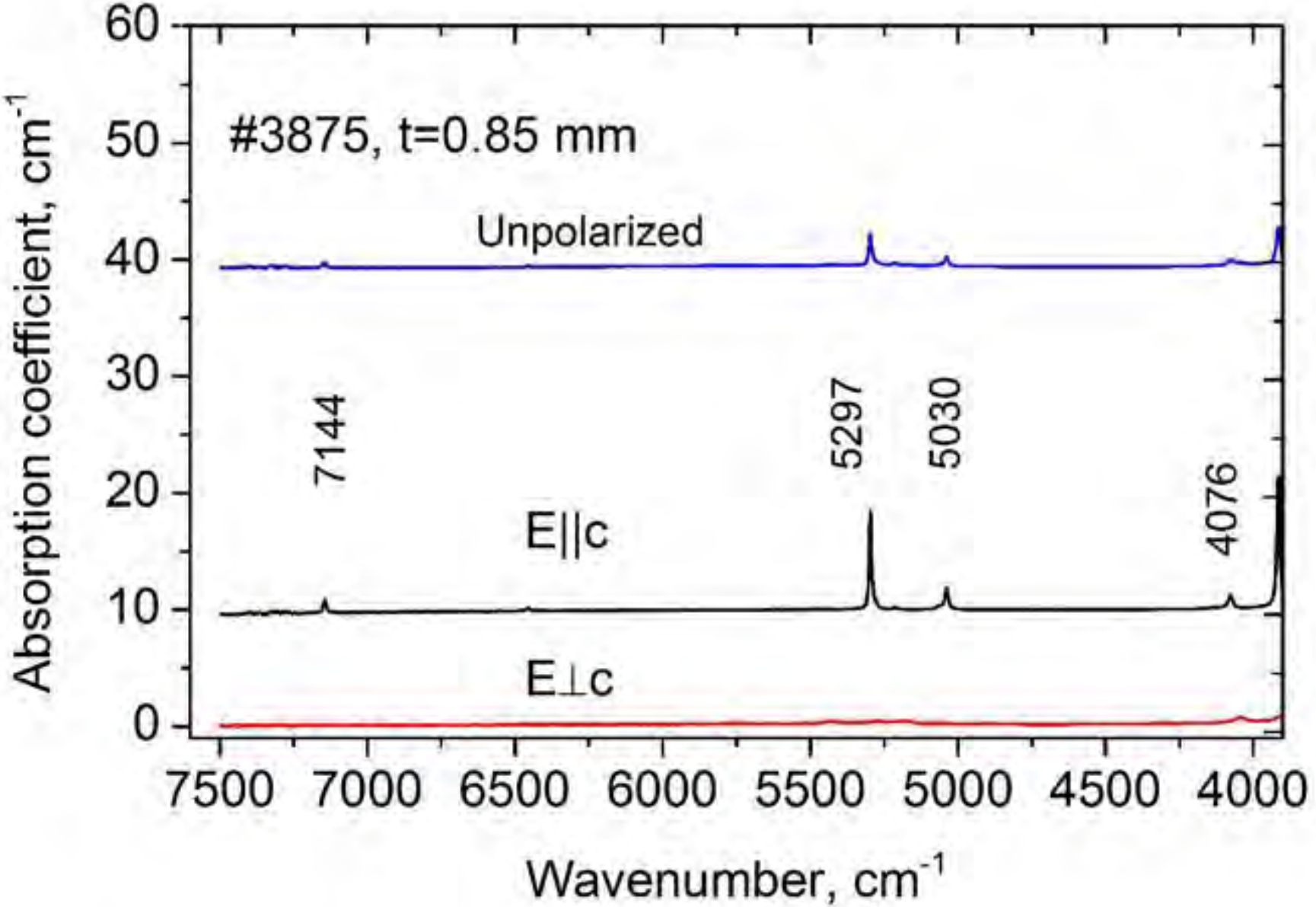
#3875, t=0.85 mm
Unpolarized
E||c
E⊥c
7144
5297
5030
4076
Absorption coefficient, cm-1
Wavenumber, cm-1
60
50
40
30
20
10
0
7500
7000
6500
6000
5500
5000
4500
4000